International Journal of Coal Geology 86 (2011) 177–189

Contents lists available at ScienceDirect

International Journal of Coal Geology

journal homepage: www.elsevier.com/locate/ijcoalgeo

A dual poroelastic model for CO_2-enhanced coalbed methane recovery

Yu Wu [a,b], Jishan Liu [b,c,*], Zhongwei Chen [b], Derek Elsworth [d], Denis Pone [e]

[a] State Key Laboratory for Geomechanics and Deep Underground Engineering, China University of Mining and Technology, Xuzhou, Jiangsu, 221008, China
[b] School of Mechanical Engineering, The University of Western Australia, WA, 6009, Australia
[c] State Key Laboratory for Geomechanics and Deep Underground Engineering, China University of Mining and Technology, Beijing, 100083, China
[d] Department of Energy and Mineral Engineering, Penn State University, USA
[e] Conoco Phillips, Bartlesville, OK, USA

ARTICLE INFO

Article history:
Received 9 August 2010
Received in revised form 14 January 2011
Accepted 14 January 2011
Available online 22 January 2011

Keywords:
Coal swelling
Coal permeability
Dual poroelasticity
Numerical simulation

ABSTRACT

Although CO_2-enhanced coalbed methane (ECBM) recovery has been comprehensively investigated, the impact of coal matrix-fracture interactions on the evolution of coal permeability under in-situ conditions is still unclear. In prior studies on this issue, the influences of coal matrix-fracture interactions have not rigorously coupled with the binary gas transport system. In this work, general porosity and permeability models are developed to explicitly quantify the interactions between binary mixtures (CO_2 and CH_4) and dual solid media (coal matrix and fracture) under the full spectrum of mechanical conditions spanning prescribed in-situ stresses through constrained displacement. These models are implemented into a fully coupled finite element (FE) model of coal deformation, binary gas flow and transport in the matrix system, and binary gas flow and transport in the fracture system. The FE model represents important non-linear responses due to the effective stress effects that cannot be recovered where mechanical influences are not rigorously coupled with the binary gas transport system.

The FE model is applied to simulate the results of a single well injection micro-pilot test performed in the anthracitic coals of the South Qinshui basin, Shanxi Province, China. The modeled CH_4 production rates are in good agreement with the observed production history. In addition to this agreement, model results also demonstrate (1) CO_2 injection increases the total pressure gradients; (2) as the CO_2 injection progresses the partial CO_2 pressure increases while the partial CH_4 pressure decreases; (3) without CO_2 injection the CH_4 content at a specific point decreases almost linearly while with the CO_2 injection the CH_4 content at a specific point decreases exponentially; (4) without CO_2 injection the CH_4 production rate decreases linearly while with CO_2 injection the CH4 production rate increases dramatically; (5) without CO_2 injection coal permeability increases almost linearly while with CO_2 injection coal permeability decreases near exponentially; (6) CO_2 injection enhances cumulative CH_4 production and the enhancement is proportional to the injection pressure; and (7) cumulative CO_2 injection volume is also proportional to the injection pressure.

1. Introduction

CO_2-enhanced coalbed methane (CO_2-ECBM) production involves the injection of CO_2 into a coal seam to promote the desorption of chemically-bound methane (CBM) while simultaneously sequestering CO_2 in the coal seam. This process exploits the greater affinity of carbon dioxide (CO_2) to adsorb onto coal relative to methane (CH_4), resulting in the net desorption of methane and its potential recovery as a low-carbon fuel. Laboratory isotherm measurements for pure gases have demonstrated that coal can adsorb approximately twice the volume of CO_2 (on a molar basis) as CH_4 (White et al., 2005). Other laboratory experiments show that this ratio could be even larger at reservoir pressures higher than 9.6 MPa, where the gaseous CO_2 is already supercritical (Hall et al., 1994; Krooss et al., 2002). Recent research on the CO_2 sorption capacity of different ranks of United States coals has shown that this ratio may be as high as 10:1 in some low rank coals (Shi and Durucan, 2008). These observations are extremely important not only for CO_2 sequestration but also for coalbed methane production. Recent estimates of the worldwide coalbed CO_2 sequestration capacity are in the range 220 (Stevens et al., 1999) to 964 Gt (Kuuskraa and Boyer, 1992; Stauffer et al., 2009). Thus coalbeds represent significant potential sinks for anthropogenic CO_2, capable of accommodating ten to thirty five years of current fossil emissions of almost 27 Gt per year (IPCC, 2005).

Since the concept of coal seam sequestration was first proposed by Macdonald of Alberta Energy during discussions with Gunter and coworkers in 1991 (Gunter et al., 1997), a number of field CO_2-ECBM storage pilot projects have been undertaken in North America, Europe

* Corresponding author at: School of Mechanical Engineering, The University of Western Australia, WA, 6009, Australia. Tel.: +61 8 6488 7205.
E-mail address: Jishan@cyllene.uwa.edu.au (J. Liu).

0166-5162/$ – see front matter © 2011 Elsevier B.V. All rights reserved.
doi:10.1016/j.coal.2011.01.004

(Poland), China and Japan. The Allison Unit pilot, which is located in the Northern New Mexico part of the San Juan Basin, represents the world's first field trial of CO_2-ECBM in 1996 (Stevens et al., 1999). However, one of the technical obstacles faced in this technology is that the preferential sorption of CO_2 over CH_4 may result in net swelling of the coal matrix (Chikatamarla et al., 2004; Levine, 1996; Pekot and Reeves, 2002). This excess dilatational strain in the coal matrix may competitively collapse the fracture porosity, resulting in net loss of permeability and staunched rates of CO_2 injection and CH_4 production (Fokker and van der Meer, 2004; Shi and Durucan, 2004). Injection rates in the Allison Unit pilot reduced by over 40% from an initial 141×10^3 m^3/day to only 85×10^3 m^3/day in the early stages of CO_2 injection. Similar dramatic reductions in CO_2 injectivity have also been observed in other field trials and confirmed in laboratory experiments (Krooss et al., 2002; Mazumder et al., 2005).

1.1. Experimental observations

The potential impacts of differential swelling on the performance and implementation of CO_2 geological sequestration projects have been investigated through experimental, field-scale, and numerical studies. Experiments on powdered high volatile bituminous Pennsylvanian coals have shown that adsorption rate decreases with increasing grain size for all experimental conditions (Busch et al., 2004). Similarly, coal type and rank (Prusty, 2007; Robertson and Christiansen, 2005) influences the preferential sorption behavior and the evolution of permeability with these changes linked to macromolecular structure (Mazumder and Wolf, 2007). The impacts of gas components on the efficiency of enhanced methane recovery have also been investigated, indicating that the presence of the nitrogen component or flue gas in the injected gas stream is capable of improving the injectivity significantly (Durucan and Shi, 2008). The adsorption kinetics of CO_2 and CH_4 at different pressures and temperatures have been explored (Charrièrea et al., 2010). Similarly, the sorption and swelling capacities of CO_2 under supercritical conditions have been examined on various dry and water-containing coals with different pressures and temperatures (Day et al., 2008; Siemons and Busch, 2007). Distributed measurements of the sorption of CO_2 have shown temporal influences of diffusion into dual porosity media (Karacan, 2007) and the role of ambient stress in modulating swelling-induced strain (Pone et al., 2008).

1.2. Permeability and numerical models

Based on experimental observations, a variety of models have been formulated to quantify the evolution of permeability during coal swelling/shrinking. The first attempts to quantify the role of stresses on the evolution of coal-reservoir permeability assumed invariant vertical stresses and linked changes in horizontal stress with the gas pressure and the sorption strain (Gray, 1992). Permeability was computed as a function of reservoir pressure with coal-matrix shrinkage assumed directly proportional to changes in the equivalent sorption pressure. Since then, a number of theoretical and empirical permeability models have been proposed. The Seidle–Huitt Model describes the evolution of permeability assuming that all changes in permeability are caused by the sorption-induced strain alone, neglecting the elastic strain (Seidle and Huitt, 1995). Another three of the most widely used permeability models are the Palmer and Mansoori model (P&M Model), the Shi and Durucan (S&D) model, and the Advanced Resources International (ARI) model (Palmer and Mansoori, 1996; Pekot and Reeves, 2002; Shi and Durucan, 2005). The P&M model is strain-based, which means that porosity change is modulated by the change in the volume strain, and the change in permeability change is calculated from this porosity change. It is derived from an equation of linear elasticity for strain changes in porous rock assuming no change in overburden stress, that changes in porosity are small and also that the permeating fluid is highly compressible. A cubic relationship between permeability and porosity is used to evaluate changes in permeability. The S&D model is based on an idealized bundled-matchstick geometry to represent a coalbed, and uses a stress-based formulation to correlate changes in the effective horizontal stress caused by the volumetric deformation together with the cleat or pore compressibilities. This stress-based model means porosity and permeability change does not come directly from volume strain change but via the horizontal stress change. Additionally, the Biot coefficient is set to unity — requiring that the change in net stress is equal to the difference between in overburden pressure and the change in pore pressure. The ARI model describes the evolution of coal permeability using a semi-empirical correlation to account for the changes of coal porosity due to pore compressibility and matrix swelling/shrinkage (Pekot and Reeves, 2002). The ARI model is essentially equivalent to P&M model in saturated coal and where the strain versus stress fits the Langmuir isotherm (Palmer, 2009). More recently, an alternative approach has been proposed to develop an improved permeability model for CO_2-ECBM recovery and CO_2 geo-sequestration in coal seams, integrating the textural and mechanical properties to describe the anisotropy of gas permeability in coal reservoirs under confined stress conditions (Wang et al., 2009). However, although permeability models incorporating sorption-induced effects have been widely studied, these proposed studies are under the assumption of either a constant overburden load, or derived from the compressibility concept of porosity, which may provide incorrect outcomes or overestimates of permeability change (Pekot and Reeves, 2002; Robertson and Christiansen, 2007). These critical and limiting assumptions have been relaxed in new models rigorously incorporating in-situ stress conditions (Zhang et al., 2008) and are extended to rigorously incorporate CO_2–CH_4 coal–gas interactions relevant to CO_2-ECBM in this study.

Mechanical and permeability models incorporating the correct physics are essential for the accurate prediction of CO_2-ECBM recovery and CO_2 geosequestration through the use of upscaling numerical models. The effects of differential swelling on the feasibility of injection, capacity and security of long-term storage is recognized as an important uncertainty for CO_2 injected into geological sites (Korre et al., 2007; Pekot and Reeves, 2002; Stauffer et al., 2009). Additionally, the inclusion of varied sorption models including the Extended Langmuir model (ELM), the Ideal Adsorbed Solution (IAS) model and the Two-Dimensional Equation of State (2D EOS) model provide important constraints on rates and fluxes of gas uptake, and define rates of permeability change (Pan and Connell, 2009). These evolutions also include “weakening” and “plasticization” (Larsen, 2003) that may affect the evolution of the deformation modulus of coal over the extensive timescale of sequestration. Despite the complex models applied to represent the evolution of CO_2-ECBM reservoirs, few of the mentioned models include feedbacks of both stress and CH_4–CO_2 counter-diffusion on the evolution of permeability. This latter effect of counter-diffusion is significant as CO_2 replaces CH_4. This effect may be incorporated through multicomponent gas diffusion and flow in bulk coals such as the bidisperse diffusion using Maxwell–Stefan (MS) diffusion (Wei et al., 2007). This behavior has been further explored for a multi-continuum porous medium with triple porosity and dual permeability, focusing on mass exchange and the interaction of micropores, marcopores and fractures (Fathi and Akkutlu, 2008; Yi et al., 2008) but for invariant permeability and diffusivity due to stress effects. Finally, the roles of deformation and flow with two components have been investigated (Connell and Detournay, 2009). Similar numerical models have been used to investigate CO_2 injectivity, one of the most important parameters for CO_2 sequestration, including the co-injection of nitrogen to delay or suppress influences of CO_2-induced swelling (Durucan and Shi, 2008; Shi and Durucan, 2004). The presence of nitrogen has been shown capable of improving the

efficiency of gas injection significantly over pure CO_2 injection with matrix and fracture permeability and the cleat system porosity as the most sensitive parameters (Fokker and van der Meer, 2004). More recently, a fully coupled finite element (FE) model of coal deformation, gas flow and diffusion and competitive adsorption was developed to investigate the net effect on the evolution of CO_2 injectivity (Chen et al., 2010).

1.3. This study

In our previous studies, a series of single poroelastic (Zhang et al., 2008) or equivalent poroelastic models (Liu et al., 2010a, 2010b) were developed to simulate the interactions of multiple processes triggered by the injection or production of single gas. Chen et al. (2010) extended these single poroelastic models to include the flow and transport of gas mixtures (binary gases: CO_2 and CH_4). Wu et al. (2010) extended these models further to a dual poroelastic model (dual solid media — coal matrix and fracture) for single gas. As a logical extension of our previous works, the objective of this study is to develop a dual poroelastic model (dual solid media — coal matrix and fracture) for binary gases (CO_2 and CH_4). The model can be applied to explicitly quantify the interactions between binary gases and dual solid media during ECBM recovery. In this work, general porosity and permeability models are developed to explicitly quantify the interactions between binary mixtures (CO_2 and CH_4) and dual solid media (coal matrix and fracture) under the full spectrum of mechanical conditions spanning prescribed in-situ stresses through constrained displacement. These models are implemented into a fully coupled finite element (FE) model of coal deformation, binary gas flow and transport in the matrix system, and binary gas flow and transport in the fracture system. The FE model represents important non-linear responses due to the effective stress effects that cannot be recovered where mechanical influences are not rigorously coupled with the binary gas transport system.

2. Governing equations

In the following, a set of field equations for coal deformation and gas flow and transport are defined. These field equations are coupled through new porosity and permeability models for coal matrix and fractures. These derivations are based on the following assumptions:

1) Coal is a homogeneous, isotropic and elastic continuum, and the system is isothermal.
2) Strains are infinitesimal.
3) Gas contained within the pores is ideal, and its viscosity is constant under isothermal conditions.
4) Gas flow through the coal matrix is assumed to be viscous flow obeying Darcy's law (a water phase is not included in the model).
5) Gas adsorption only takes place in matrix.

In the following derivations, the coal is conceptualized as in Fig. 1. It consists of coal matrix and fractures. The cubic matrix length and the fracture aperture are represented by a and b, respectively. K_n is the fracture stiffness, and σ_e the effective stress.

2.1. Kinetics of gas adsorption

Based on the assumption of an ideal gas, the equation of state for gas in the fracture and matrix can be defined as:

$$pV = n{\cdot}RT. \tag{1}$$

The gas concentration is defined as:

$$C = \frac{n}{V} = \frac{p}{RT} \tag{2}$$

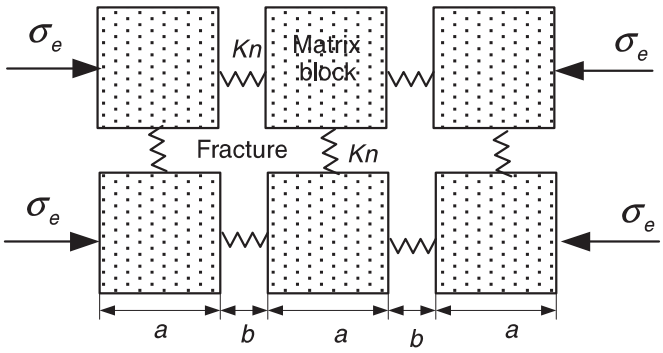

Fig. 1. Representation of coal as a dual poroelastic medium.

where, C is the gas concentration, mol/m^3, defined as the number of moles, n, per unit volume, V, p is gas pressure, R is the gas constant, m$^3\cdot$Pa/K$\cdot$mol and T is temperature, K.

For a multi-component gas system, the concentration of gas i can be expressed as:

$$C_i = \frac{p}{RT}\cdot x_i \tag{3}$$

where, x_i is the partial pressure coefficient. Accordingly, the density of the multi-component gas is defined as:

$$\rho_g = \sum_{i=1}^{j} C_i{\cdot}M_i \tag{4}$$

where, M_i is the molar mass of component i.

Based on previous assumption (5), the gas only adsorbs to the coal grains within the matrix. According to the isothermal Langmuir sorption relation, the gas volume adsorbed per unit coal mass can be calculated by using Eq. (5) (Langmuir, 1916).

$$V = \frac{V_L p_m}{p_m + p_L}. \tag{5}$$

Substituting Eq. (3) into Eq. (5) gives the extended Langmuir isotherm (ELI):

$$V_k = \frac{V_{k0}C_k b'_k}{1 + \sum_{j=1}^{N} C_j b'_j.} \tag{6}$$

For a binary mixture of CO_2 (component 1) and CH_4 (component 2), Eq. (6) is used to calculate the total amount of gas adsorbed to the coal at any given pressure:

$$V_t = \sum_{k=1}^{2} V_k = \frac{V_{10}C_1 b'_1 + V_{20}C_2 b'_2}{1 + C_1 b'_1 + C_2 b'_2} \tag{7}$$

where, b'_i represents the Langmuir pressure constant of component i, $b' = 1/p_L$ and V_{i0} represents the Langmuir volume constant of component i.

Experimental evidence (Butler and Ockrent, 1930; Do, 1998) supports the use of the extended Langmuir isotherm equation in representing the adsorption of gas mixtures. By analogy, the sorption-induced volumetric strain due to each gas species can be computed as

$$\varepsilon_k = \varepsilon_{Lk}\frac{C_k b'_k}{1 + \sum_{j=1}^{n} C_j b'_j.} \tag{8}$$

The total sorption-induced strain is determined by summing the strains caused by each gas species, as,

$$\varepsilon_s = \sum_{k=1}^{n} \varepsilon_k = \sum_{k=1}^{n} \varepsilon_{Lk} \frac{C_k b'_k}{1 + \sum_{j=1}^{n} C_j b'_j}. \tag{9}$$

2.2. Permeability models for matrix and fracture

Based on our previous work (Liu et al., 2010a, 2010b; Wu et al., 2009, 2010), the porosity and permeability model for the coal matrix can be defined as:

$$\phi_m = \phi_{m0} - \frac{\alpha}{K} \cdot \frac{1}{\frac{b_0}{aK_f} + \frac{1}{K}} \left(\frac{\varepsilon_L P_m}{P_L + P_m} - \varepsilon_v \right) \tag{10}$$

$$\frac{k_m}{k_{m0}} = \left(1 - \frac{\alpha}{\phi_{m0} K} \cdot \frac{1}{\frac{b_0}{aK_f} + \frac{1}{K}} \left(\frac{\varepsilon_L P_m}{P_L + P_m} - \varepsilon_v \right) \right)^3. \tag{11}$$

These two equations are for the case of a single gas. Substituting the total volumetric strain for the case of a binary gas mixture (Eq. (9)) into Eqs. (10) and (11) yields the matrix porosity and permeability models as

$$\phi_m = \phi_{m0} - \frac{\alpha}{K} \cdot \frac{1}{\frac{b_0}{aK_f} + \frac{1}{K}} \left(\sum_{k=1}^{2} \varepsilon_{Lk} \frac{C_{mk} b'_k}{1 + \sum_{j=1}^{2} C_{mj} b'_j} - \varepsilon_v \right) \tag{12}$$

$$\frac{k_m}{k_{m0}} = \left(1 - \frac{\alpha}{\phi_{m0} K} \cdot \frac{1}{\frac{b_0}{aK_f} + \frac{1}{K}} \left(\sum_{k=1}^{2} \varepsilon_{Lk} \frac{C_{mk} b'_k}{1 + \sum_{j=1}^{2} C_{mj} b'_j} - \varepsilon_v \right) \right)^3. \tag{13}$$

In those equations, the subscript 1 represents CO_2, subscript 2 represents CH_4, subscript 0 represents the initial state for each gas component and subscript m represents the matrix. α is the Biot coefficient for the coal matrix (Biot, 1941). K is the matrix bulk modulus $K = \frac{E}{1-2\nu}$, K_f is the modified fracture stiffness $K_f = b_0 K_n$ and K_n is the fracture stiffness.

Similarly, the porosity and permeability model for the fracture system can be derived as

$$\frac{\phi_f}{\phi_{f0}} = 1 + \frac{\Delta b}{b_0} = 1 - \frac{3}{\phi_{f0} + \frac{3K_f}{K}} \left(\alpha_T \Delta T + \sum_{k=1}^{2} \varepsilon_L \frac{C_{mk} b'_k}{1 + \sum_{j=1}^{2} C_{mj} b'_j} - \varepsilon_v \right) \tag{14}$$

$$\frac{k_f}{k_{f0}} = \left(1 + \frac{\Delta b}{b_0} \right)^3 = \left(1 - \frac{3}{\phi_{f0} + \frac{3K_f}{K}} \left(\alpha_T \Delta T + \sum_{k=1}^{2} \varepsilon_{Lk} \frac{C_{mk} b'_k}{1 + \sum_{j=1}^{2} C_{mj} b'_j} - \varepsilon_v \right) \right)^3 \tag{15}$$

where, subscript f represents that the parameter relates to the fracture.

If the model is constrained on all four sides and injection is isothermal then the porosity and permeability models can be rewritten as

$$\frac{\phi_f}{\phi_{f0}} = 1 - \frac{3}{\phi_{f0} + \frac{3K_f}{K}} \left(\sum_{k=1}^{2} \varepsilon_{Lk} \frac{C_{mk} b'_k}{1 + \sum_{j=1}^{2} C_{mj} b'_j} \right) \tag{16}$$

$$\frac{k_f}{k_{f0}} = \left(1 - \frac{3}{\phi_{f0} + \frac{3K_f}{K}} \left(\sum_{k=1}^{2} \varepsilon_{Lk} \frac{C_{mk} b'_k}{1 + \sum_{j=1}^{2} C_{mj} b'_j} \right) \right)^3 \tag{17}$$

For the anisotropic case, the directional permeabilities can be defined as

$$\begin{cases} \frac{k_{fx}}{k_{f0}} = \frac{1}{2} \left(1 - \frac{1}{\phi_{f0} + \frac{3K_f}{K}} \left(\alpha_T \Delta T + \sum_{k=1}^{2} \varepsilon_{Lk} \frac{C_{mk} b'_k}{1 + \sum_{j=1}^{2} C_{mj} b'_j} - 3\varepsilon_y \right) \right)^3 \\ \qquad + \frac{1}{2} \left(1 - \frac{1}{\phi_{f0} + \frac{3K_f}{K}} \left(\alpha_T \Delta T + \sum_{k=1}^{2} \varepsilon_{Lk} \frac{C_{mk} b'_k}{1 + \sum_{j=1}^{2} C_{mj} b'_j} - 3\varepsilon_z \right) \right)^3 \\ \frac{k_{fy}}{k_{f0}} = \frac{1}{2} \left(1 - \frac{1}{\phi_{f0} + \frac{3K_f}{K}} \left(\alpha_T \Delta T + \sum_{k=1}^{2} \varepsilon_{Lk} \frac{C_{mk} b'_k}{1 + \sum_{j=1}^{2} C_{mj} b'_j} - 3\varepsilon_x \right) \right)^3 \\ \qquad + \frac{1}{2} \left(1 - \frac{1}{\phi_{f0} + \frac{3K_f}{K}} \left(\alpha_T \Delta T + \sum_{k=1}^{2} \varepsilon_{Lk} \frac{C_{mk} b'_k}{1 + \sum_{j=1}^{2} C_{mj} b'_j} - 3\varepsilon_z \right) \right)^3 \\ \frac{k_{fz}}{k_{f0}} = \frac{1}{2} \left(1 - \frac{1}{\phi_{f0} + \frac{3K_f}{K}} \left(\alpha_T \Delta T + \sum_{k=1}^{2} \varepsilon_{Lk} \frac{C_{mk} b'_k}{1 + \sum_{j=1}^{2} C_{mj} b'_j} - 3\varepsilon_x \right) \right)^3 \\ \qquad + \frac{1}{2} \left(1 - \frac{1}{\phi_{f0} + \frac{3K_f}{K}} \left(\alpha_T \Delta T + \sum_{k=1}^{2} \varepsilon_{Lk} \frac{C_{mk} b'_k}{1 + \sum_{j=1}^{2} C_{mj} b'_j} - 3\varepsilon_y \right) \right)^3. \end{cases} \tag{18}$$

Eq. (18) is the general permeability model for CO_2-ECBM. It quantifies the interactions between the two gas components, CO_2 and CH_4, and the two solid components of fracture and matrix, as shown in Fig. 2.

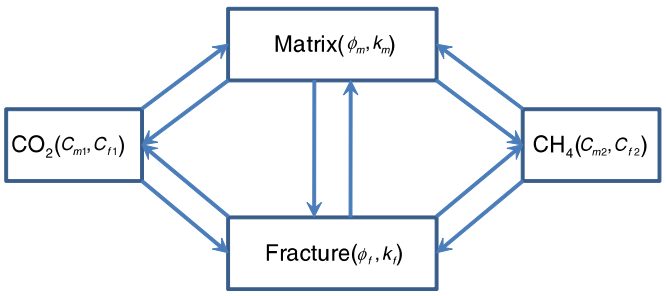

Fig. 2. The interactions between binary gas, fracture and matrix.

These interactions are highly complex. On one hand, CO_2 injection increases the total pressure in the coal and the pressure gradient between fracture and matrix also increases. This will accelerate the CO_2 adsorption on the coal grain and the CH_4 desorption from the coal grain. But on the other hand, the fracture permeability decreases with the CO_2 adsorption because of the swelling of coal grain, and increases with desorption because of the shrinking of coal grain. The net change could be positive (permeability gain) or negative (permeability loss) depending on the constraint conditions applied to the model. Whether the end result is permeability gain or loss is controlled by field equations as defined in the following section.

3. Field equations

3.1. Coal deformation

Coal deformation is defined through the Navier equation for linear poroelastic media, accommodating pore pressure and absorption/desorption induced effects as additional source terms acting as additional body forces. According to assumption (1), the strain-displacement relation is defined as

$$\varepsilon_{ij} = \frac{1}{2}\left(u_{i,j} + u_{j,i}\right) \tag{19}$$

and the equilibrium equation is defined as

$$\sigma_{ij,j} + f_i = 0 \tag{20}$$

where ε_{ij} is the component of the total strain tensor, u_i is the component of the displacement, σ_{ij} denotes the component of the total stress tensor and f_i denotes the component of the body force. Accommodating the influences of pore pressure and sorption-induced strain (Detournay and Cheng, 1993; Zhang et al., 2008), the constitutive relation for the deformable dual porosity coal seam (Bai and Elsworth, 2000; Elsworth and Bai, 1992; Wu et al., 2010) becomes

$$\varepsilon_{ij} = \frac{1}{2G}\sigma_{ij} - \left(\frac{1}{6G} - \frac{1}{9K}\right)\sigma_{kk}\delta_{ij} + \frac{\alpha}{3K}p_m\delta_{ij} + \frac{\beta}{3a\cdot Kn}p_f\delta_{ij} + \frac{\varepsilon_s}{3}\delta_{ij} \tag{21}$$

where $G = \frac{E_e}{2(1+\nu)}$, $K = \frac{E_e}{3(1-2\nu)}$, $E_e = \frac{1}{1/E + 1/(K_n\cdot a)}$, $\alpha = 1 - \frac{K}{K_s}$, $\beta = 1 - \frac{K}{K_n\cdot a}$. K and K_s represent the bulk modulus of coal and coal grains respectively, G is the shear modulus of coal, E is the Young's modulus of coal, ν is the Poisson ratio of coal, α, β are the Biot coefficients (Biot, 1941) and δ_{ij} is the Kronecker delta. p_m and p_f are the total pressure in the matrix and fracture respectively (the usual dual porosity construct) but with each also comprising the summed influence of the two components of the binary mixture.

According to the equation of state (EOS) for the binary gas, each partial pressure (p_k) and the total pressure (p) for the binary flow system can be expressed as

$$p_k = C_k \cdot RT \cdot z_k \tag{22}$$

$$p_m = \sum_{k=1}^{2} C_{mk} \cdot RT \cdot z_{mk} \tag{23}$$

$$p_f = \sum_{k=1}^{2} C_{fk} \cdot RT \cdot z_{fk} \tag{24}$$

where z_k is the correction factor that accounts for the non-ideal behavior of the gas, which changes with pressure and temperature, and R and T again represent the universal gas constant and absolute temperature, respectively.

Combining Eqs. (19)–(24) yields the Navier-type equation expressed as

$$Gu_{i,kk} + \frac{G}{1-2\nu}u_{k,ki} = (\alpha\cdot RT + K\cdot AA)C_{m1,i} + (\alpha\cdot RT + K\cdot BB)C_{m2,i} + \beta\cdot RT\cdot\left(C_{f1,i} + C_{f2,i}\right) - f_i \tag{25}$$

where

$$AA = \frac{\varepsilon_{L1}b_1'(1 + b_2'C_{m2})}{(1 + C_{m1}b_1' + C_{m2}b_2')^2} - \frac{\varepsilon_{L2}b_1'b_2'C_{m2}}{(1 + C_{m1}b_1' + C_{m2}b_2')^2} \tag{26}$$

$$BB = \frac{\varepsilon_{L2}b_2'(1 + b_1'C_{m1})}{(1 + C_{m1}b_1' + C_{m2}b_2')^2} - \frac{\varepsilon_{L1}b_1'b_{2Cm1}'}{(1 + C_{m1}b_1' + C_{m2}b_2')^2.} \tag{27}$$

Both terms on the left side of Eq. (25) represent the elastic deformation of the system influenced by equivalent fluid pressure and sorption-induced body forces. The first two terms on the right side of Eq. (25) represent the effects of pore pressure and gas adsorptions in the matrix. The third term represents the effects of pore pressure in the fracture. The fourth term represents a generic body force within the porous medium system, typically accommodating self-weight of the medium.

3.2. Binary gas transport

The binary transport of gas in this system includes three pathways, in decreasing order of transport rapidity, these are: (i) Darcy flow through cleats and cracks; (ii) Fickian diffusion through the coal matrix to reach the coal pores; and (iii) Case II diffusion, in which the rate-determining step is the motion of the coal macromolecules (Goodman et al., 2005; Karacan, 2003). The mass balance equation can be expressed for a static medium incorporating these convective and diffusive modes of transport but involving the interchange between free and adsorbed gas as

$$\frac{\partial m_k}{\partial t} + \nabla\cdot\left(\vec{v}\cdot\rho_{gk}\right) + \nabla\cdot\left(-D_k\cdot\nabla m_{kf}\right) = Q_{sk} \tag{28}$$

where m_k is the gas content of gas component k, including free-phase gas and absorbed gas. The mass of each component of fracture and matrix contained in a unit volume of coal can be defined as

$$m_{fk} = \phi_f \cdot C_{fk}M_{fk} \tag{29}$$

$$m_{mk} = \phi_m \cdot C_{mk}M_{mk} + (1-\phi_{m0})\cdot\rho_c\cdot\rho_{sg}\frac{V_{Lk}b_k'C_{mk}}{1 + C_{m1}b_1' + C_{m2}b_2'} \tag{30}$$

where $\vec{v}$ is the vector of convective velocity, determined by the injection gas concentration gradient, and can be expressed as

$$\vec{v_f} = -\frac{k_fRT}{\mu}\nabla C_{f2} \tag{31}$$

$$\vec{v_m} = -\frac{k_mRT}{\mu}\nabla C_{m2} \tag{32}$$

where ρ_{gk} is the gas density, ρ_{sg} is the gas density at standard conditions, ρ_c is the coal density, M_k is the molar mass of component k, Q_{sk} is the gas source or sink, and D_k is the hydrodynamic dispersion coefficient defined as

$$D_{fk} = \beta_c\cdot\vec{v_f} + D_{fk0} \tag{33}$$

$$D_{mk} = \beta_c\cdot\vec{v_m} + D_{mk0} \tag{34}$$

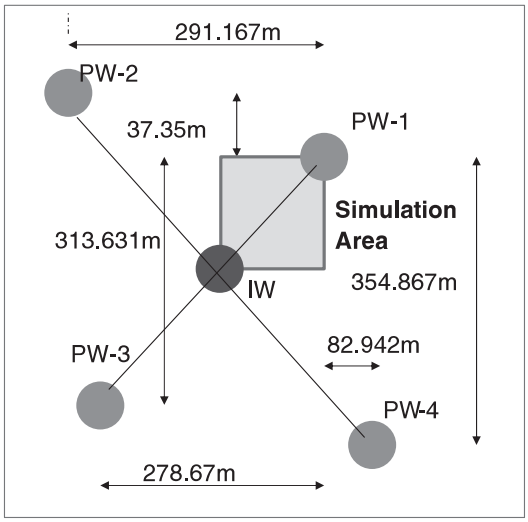

Fig. 3. Pattern configuration of the multi-well pilot testing (Wong et al., 2007).

Table 1
Modeling parameters for the numerical simulation.

Parameter	Value
Young's modulus of coal (E, GPa)	2.71
Young's modulus of coal grains (E_s, GPa)	8.13
Poisson's ratio of coal (ν)	0.34
Density of coal (ρ_c, kg/m^3)	1.25×10^3
Gas dynamic viscosity (μ, Pa s)	1.84×10^{-5}
CO_2 Langmuir volume constant (V_{L1}, m^3/kg)	0.0477
CH_4 Langmuir volume constant (V_{L2}, m^3/kg)	0.0256
CO_2 Langmuir volumetric strain constant (ε_{L1})	0.0237
CH_4 Langmuir volumetric strain constant (ε_{L2})	0.0128
CH_4 Langmuir pressure constant (MPa)	2.07
CO_2 Langmuir pressure constant (MPa)	1.38
Initial porosity of matrix(ϕ_{m0})	0.0423
Initial porosity of fracture (ϕ_{f0})	0.001
Initial permeability of matrix (k_{m0}, m^2)	3.0×10^{-16}
Initial permeability of fracture (k_{f0}, m^2)	1.0×10^{-14}
CH_4 Diffusion Coefficient (m^2/s)	3.6×10^{-12}
CO_2 Diffusion Coefficient (m^2/s)	5.8×10^{-12}

where D_{k0} is the coefficient of molecular diffusion of component k and β_c is the dynamic dispersivity.

Combining Eqs. (28) through (30) yields the flow equation in the matrix as

$$C_{mk}\frac{\partial\phi_m}{\partial t}+\phi_f\frac{\partial C_{mk}}{\partial t}+\frac{\partial C_m}{\partial t}\left[(1-\phi_{m0})\cdot\rho_c\cdot\rho_{sg}\frac{V_{Lk}b_k'C_{mk}}{1+C_{m1}b_1'+C_{m2}b_2'}\right]$$
$$=-\nabla\cdot\left[-\frac{k_fRT}{\mu}C_{mk}\cdot\nabla C_{mk}\right]+\nabla\cdot\left[-D_f\phi_f\cdot\nabla C_{mk}\right] \quad (35)$$
$$-8\left(1+\frac{1}{a^2}\right)\left(C_{fk}-C_{mk}\right).$$

From Eq. (12) , the partial derivative of ϕ_m with respect to time is expressed as

$$\frac{\partial\phi_m}{\partial t}=-\frac{\alpha}{K}\cdot\frac{1}{\frac{b_0}{aK_f}+\frac{1}{K}}\frac{\partial\varepsilon_s}{\partial t}+\frac{\alpha}{K}\cdot\frac{1}{\frac{b_0}{aK_f}+\frac{1}{K}}\frac{\partial\varepsilon_v}{\partial t}$$
$$=-\frac{\alpha}{K}\cdot\frac{1}{\frac{b_0}{aK_f}+\frac{1}{K}}\left(AA\cdot\frac{\partial C_{m1}}{\partial t}+BB\cdot\frac{\partial C_{m2}}{\partial t}\right)+\frac{\alpha}{K}\cdot\frac{1}{\frac{b_0}{aK_f}+\frac{1}{K}}\frac{\partial\varepsilon_v}{\partial t}. \quad (36)$$

Substituting Eqs. (36) into (35), and separating for each gas component yields the governing equations of flows for a binary mixture of CO_2 (component 1) and CH_4 (component 2) in the matrix

$$\left[\phi_m+(1-\phi_m)\cdot\frac{\rho_cp_{at}}{RT}\cdot CC-\frac{\alpha K_f}{\frac{b_0}{a}K+K_f}\cdot C_{m1}\cdot AA\right]\frac{\partial C_{m1}}{\partial t}$$
$$+\left[-\frac{\alpha K_f}{\frac{b_0}{a}K+K_f}\cdot C_{m1}\cdot BB-(1-\phi_m)\cdot\frac{\rho_cp_{at}}{RT}\cdot DD\right]\frac{\partial C_{m2}}{\partial t} \quad (37)$$
$$+\frac{\alpha K_f}{\frac{b_0}{a}K+K_f}\cdot C_{m1}\frac{\partial\varepsilon_v}{\partial t}=\nabla\cdot[D_{m1}\phi_m\cdot\nabla C_{m1}]-\nabla\cdot\left[-\frac{k_mRT}{\mu}C_{m1}\cdot\nabla C_{m2}\right]$$
$$+8\left(1+\frac{1}{a^2}\right)\left(C_{f1}-C_{m1}\right)$$

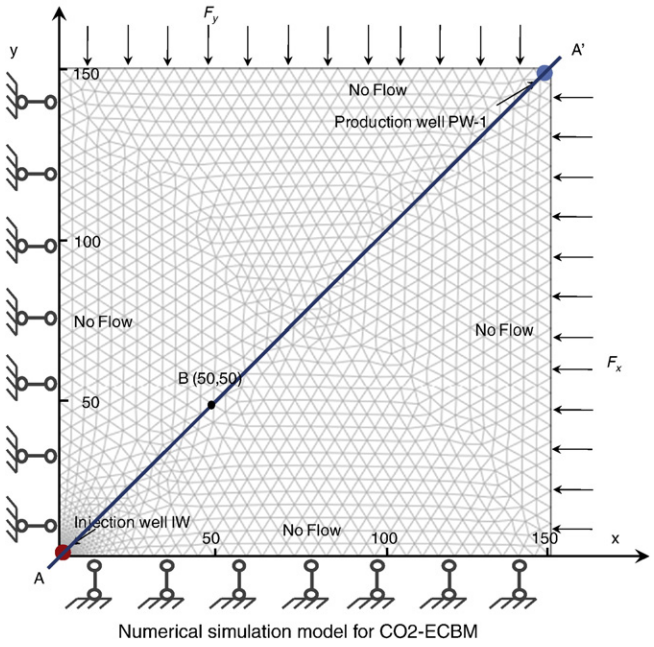

Fig. 4. Numerical simulation model for CO2-ECBM.

Table 2
Simulation models.

Index	Technology	Injection pressure
Model 1	CBM	No injection
Model 2	CO_2-ECBM	4 MPa
Model 3	CO_2-ECBM	8 MPa

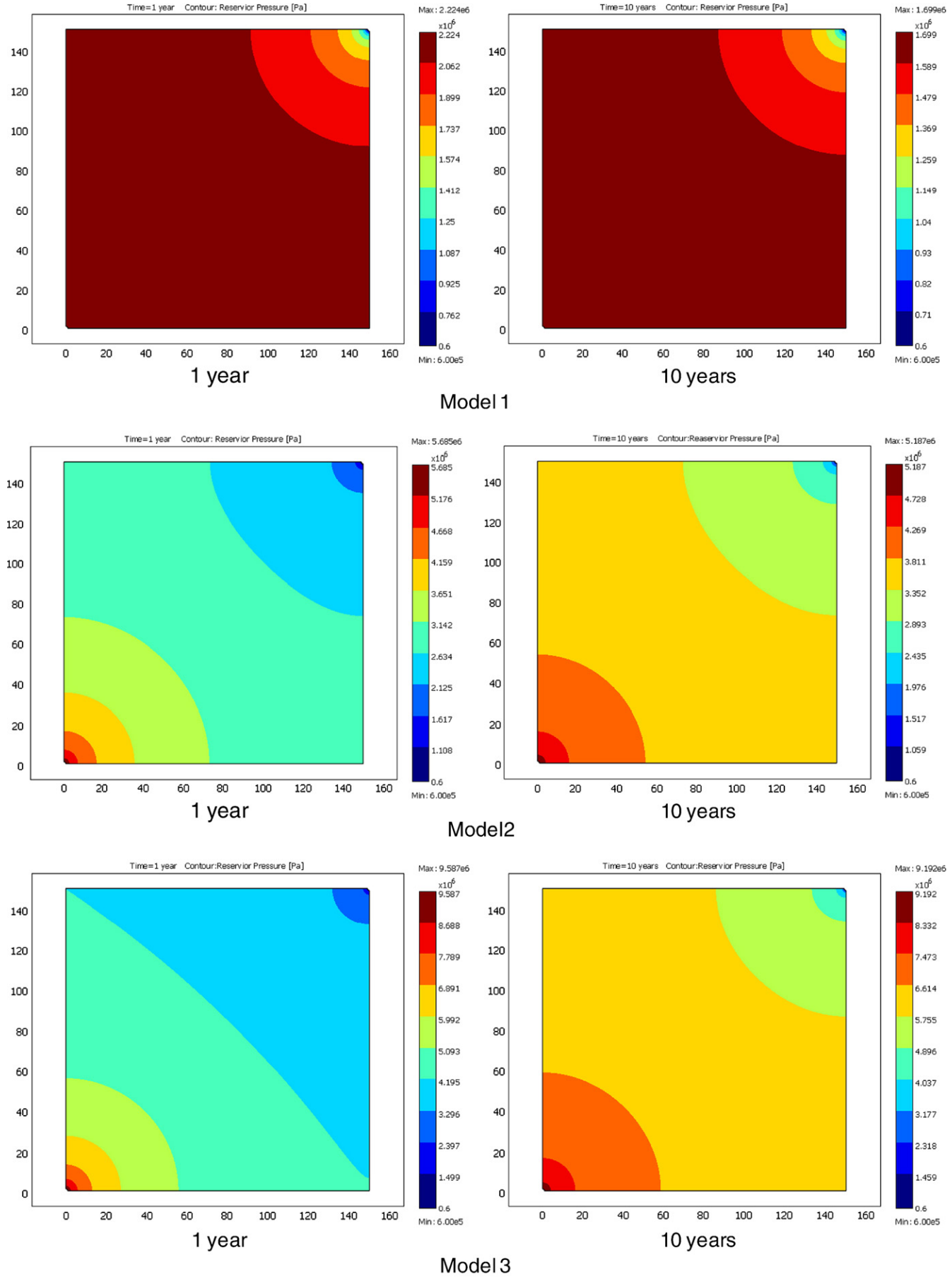

Fig. 5. Distribution of the total pressure: Model 1 — CBM Only; Model 2 — CO_2-ECBM with an Injection Pressure of 4 MPa; Model 2 — CO_2-ECBM with an Injection Pressure of 8 MPa.

$$\left[\phi_m - \frac{\alpha K_f}{\frac{b_0}{a}K + K_f}\cdot C_{m2}\cdot BB + (1-\phi_m)\cdot\frac{\rho_c p_{at}}{RT}\cdot C'C'\right]\frac{\partial C_{m2}}{\partial t}$$
$$+\left[-\frac{\alpha K_f}{\frac{b_0}{a}K + K_f}C_{m1}\cdot AA - (1-\phi_m)\cdot\frac{\rho_c p_{at}}{RT}\cdot D'D'\right]\frac{\partial C_{m1}}{\partial t} \quad (38)$$
$$+\frac{\alpha K_f}{\frac{b_0}{a}K + K_f}\cdot C_{m2}\frac{\partial \varepsilon_v}{\partial t} = \nabla\cdot[D_{m2}\phi_m\cdot\nabla C_{m2}]$$
$$-\nabla\cdot\left[-\frac{k_m RT}{\mu}C_{m2}\cdot\nabla C_{m2}\right] + 8\left(1+\frac{1}{a^2}\right)\left(C_{f2}-C_{m2}\right)$$

where $CC = \frac{V_{L1}b_1'(1+b_2'C_{m2})}{(1+C_{m1}b_1'+C_{m2}b_2')^2}$, $DD = \frac{V_{L1}b_1'b_2'C_{m1}}{(1+C_{m1}b_1'+C_{m2}b_2')^2}$, $C'C' = \frac{V_{L2}b_2'(1+b_1'C_{m1})}{(1+C_{m1}b_1'+C_{m2}b_2')^2}$, $D'D' = \frac{V_{L2}b_1'b_2'C_{m2}}{(1+C_{m1}b_1'+C_{m2}b_2')^2}$.

Similarly, the flow equation in the fracture system can be defined by combining Eqs. (28) through (29) to yield the flow equation

$$C_{fk}\frac{\partial\phi_f}{\partial t} + \phi_f\frac{\partial C_{fk}}{\partial t} + \nabla\cdot\left[-\frac{k_f RT}{\mu}C_{fk}\cdot\nabla C_{f2}\right] + \nabla\cdot\left[-D_{fk}\phi_f\cdot\nabla C_{fk}\right]$$
$$= -8\left(1+\frac{1}{a^2}\right)\left(C_{fk}-C_{mk}\right). \quad (39)$$

From Eq. (14) , the partial derivative of ϕ_f with respect to time is expressed as

$$\frac{\partial\phi_f}{\partial t} = -\phi_{f0}\frac{3}{\phi_{f0}+\frac{3K_f}{K}}\frac{\partial\varepsilon_s}{\partial t} + \phi_{f0}\frac{3}{\phi_{f0}+\frac{3K_f}{K}}\frac{\partial\varepsilon_v}{\partial t}$$
$$= -\phi_{f0}\frac{3}{\phi_{f0}+\frac{3K_f}{K}}\left(AA\cdot\frac{\partial C_{m1}}{\partial t} + BB\cdot\frac{\partial C_{m2}}{\partial t}\right) + \phi_{f0}\frac{3}{\phi_{f0}+\frac{3K_f}{K}}\frac{\partial\varepsilon_v}{\partial t}. \quad (40)$$

Substituting Eqs. (40) into (39), and separating for each gas component yields the governing equations of flow for binary mixture of CO_2 (component 1) and CH_4 (component 2) in the fracture

$$\phi_f\frac{\partial C_{f1}}{\partial t} - \phi_{f0}\frac{3C_{f1}}{\phi_{f0}+\frac{3K_f}{K}}\left(AA\cdot\frac{\partial C_{m1}}{\partial t} + BB\cdot\frac{\partial C_{m2}}{\partial t}\right) + \phi_{f0}\frac{3C_{f1}}{\phi_{f0}+\frac{3K_f}{K}}\frac{\partial\varepsilon_v}{\partial t}$$
$$= -8\left(1+\frac{1}{a^2}\right)\left(C_{f1}-C_{m1}\right) - \nabla\cdot\left[-\frac{k_f RT}{\mu}C_{f1}\cdot\nabla C_{f2}\right] + \nabla\cdot\left[D_{f1}\phi_f\cdot\nabla C_{f1}\right] \quad (41)$$

$$\phi_f\frac{\partial C_{f2}}{\partial t} - \phi_{f0}\frac{3C_{f2}}{\phi_{f0}+\frac{3K_f}{K}}\left(AA\cdot\frac{\partial C_{m2}}{\partial t} + BB\cdot\frac{\partial C_{m2}}{\partial t}\right) + \phi_{f0}\frac{3C_{f2}}{\phi_{f0}+\frac{3K_f}{K}}\frac{\partial\varepsilon_v}{\partial t}$$
$$= -8\left(1+\frac{1}{a^2}\right)\left(C_{f2}-C_{m2}\right) - \nabla\cdot\left[-\frac{k_f RT}{\mu}C_{f2}\cdot\nabla C_{f2}\right] + \nabla\cdot\left[D_{f2}\phi_f\cdot\nabla C_{f2}\right]. \quad (42)$$

In Eq. (37), the summation of the first three terms (related to $\partial C_{m1}/\partial t$) on the left side represent the resultant volume of gas sequestered to storage per unit change in the concentration of CO_2 in per unit volume of the reservoir. These three contributing components are, in order: (i) the volume of gas released (or sequestered) from the free-phase gas; (ii) the volume of gas released (or sequestered) from the adsorbed-phase gas; and (iii) the volume of gas released (or sequestered) due to deformation of the coal gains. The summation of the following two terms on the left side (related to $\partial C_{m2}/\partial t$) represent the resultant volume of gas released from storage per unit change in the concentration of CH_4 in per unit volume of the reservoir. These two contributing components are, in order: (i) the volume of gas released (or sequestered) due to coal gain deformation; and (ii) the volume of gas released (or sequestered) from the adsorped-phase gas. The last term on the left side is the volume of gas released (or sequestered) due to the bulk (skeletal) deformation of the coal. On the right-hand side, the first term represents the mass change rate due to diffusion while the second term represents the mass change rate due to flow. The last term is the mass exchange between matrix and fracture system. Similar explanations apply to Eq. (38) representing the transport of CH_4.

Therefore , Eqs. (37), (38), (41), (42) define the coupled gas flow and coal deformation model with diffusion of a binary gas mixture in a dual-porosity medium. These field equations have been implemented into and solved by COMSOL Multiphysics.

4. Example of a field application

CBM recovery triggers a series of coal–gas interactions. For primary gas production, the reduction of gas pressure increases effective stress which in turn closes the apertures of fractures and reduces the permeability. As the gas pressure reduces below the desorption point, methane is released from the coal matrix to the fracture network and the coal matrix shrinks. As a direct consequence of this matrix shrinkage the fractures dilate and fracture permeability correspondingly increases. Thus a rapid initial reduction in fracture permeability (due to change in effective stress) is supplanted by a slow increase in permeability (with matrix shrinkage). Whether the ultimate, long-term, permeability is greater or less than the initial permeability depends on the net influence of these dual competing mechanisms. CO_2-ECBM is a relatively new concept and only a few pilot tests have been conducted (Bergen et al., 2009; Fujioka et al., 2010; Wong et al., 2007, 2010). In the following section, the CO_2-ECBM model developed in the preceding is used to simulate the results of a single well micro-pilot test performed at an existing well in the anthracite coals of the South Qinshui basin, Shanxi Province, China.

4.1. Model description

The coalbed methane reserve in the Qinshui Basin of Shanxi province, China has estimated has an estimated reserve of about 3.28×10^{12} m^3 of methane at standard conditions. Because of this large reserve, the Southeast Qinshui Basin has become a favoured area for the exploration and development of CBM. More than 70 coalbed methane wells have been drilled in this region by the China United Coalbed Methane Company and the China National Petroleum

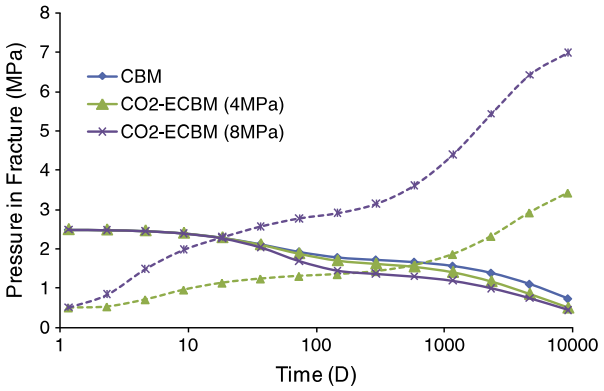

Fig. 6. Evolution of the partial pressure at point B for three different simulation models.

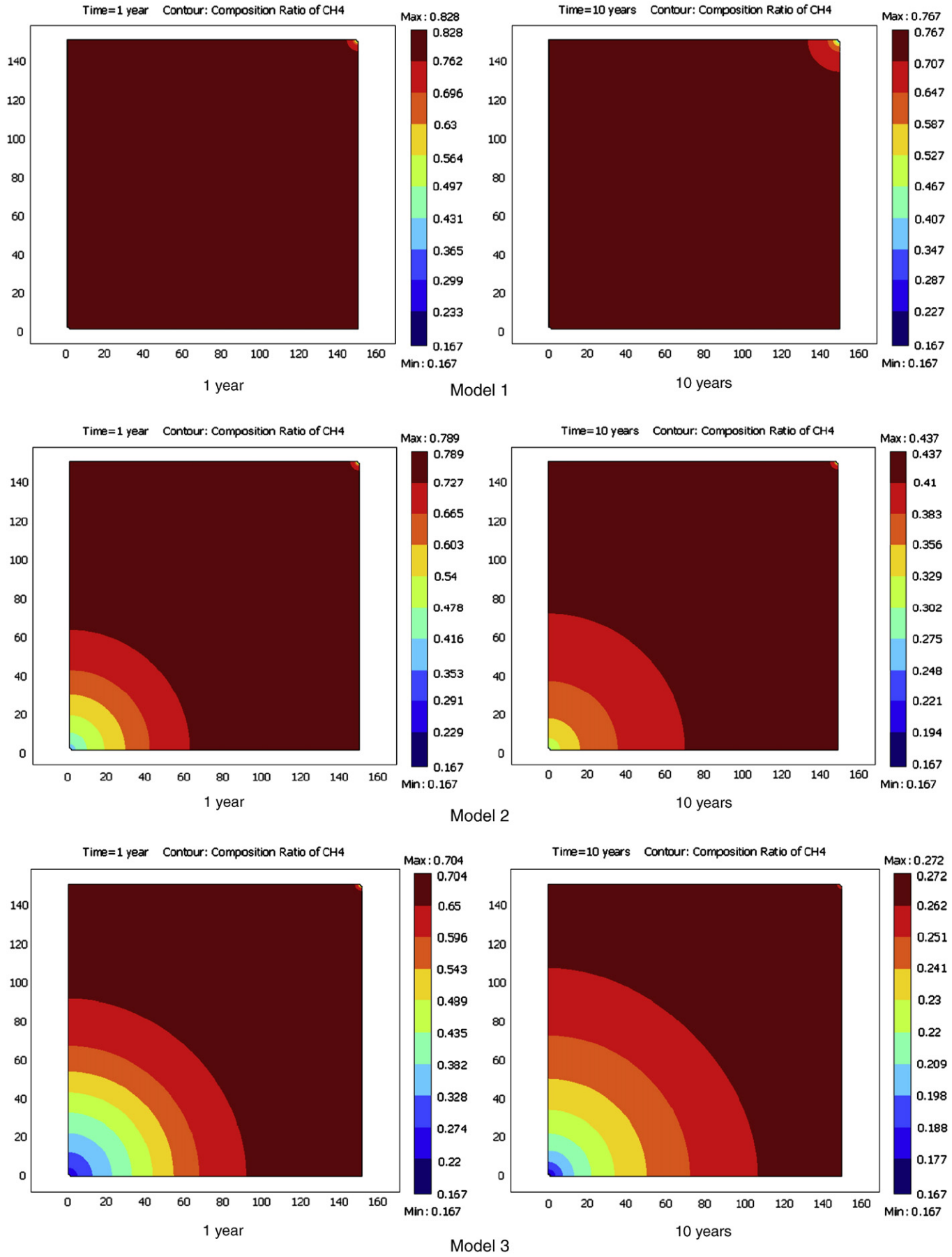

Fig. 7. The distribution of CH_4 content in the matrix.

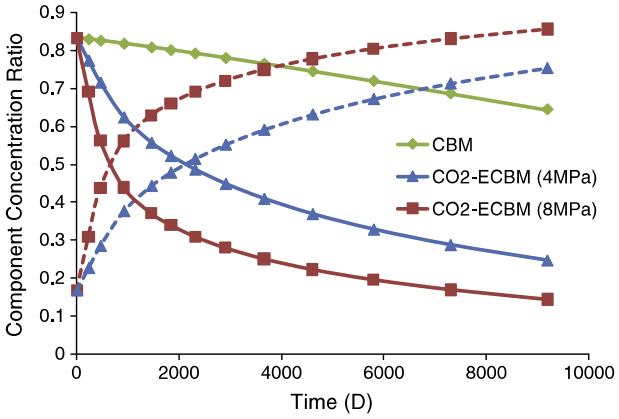

Fig. 8. Evolution of CO_2 and CH_4 contents at point B within the matrix.

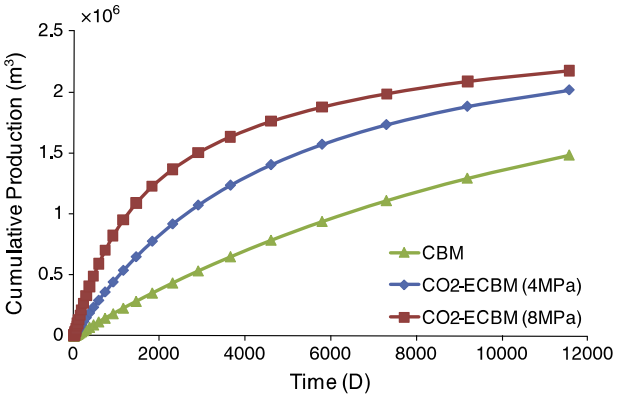

Fig. 10. Cumulative CH_4 production from a single well for the three different models.

Corporation. The highest coalbed methane production rate is 16,000 m^3/d per well, and the average is 2000–4000 m^3/d per well. The exploration confirms that CBM reservoirs with high permeability exist in the Southeast Qinshui Basin, which is the first basin to be developed commercially in China (Su et al., 2005). In 2002, pilot testing of CO_2-ECBM in a deep unminable coalbed was undertaken jointly by the Chinese Commerce Department and the Canadian International Development Agency (CIDA). Fig. 3 shows the configuration of the multi-wells pilot testing — a central injection well is centered within a near-square array of four production wells in a traditional five-spot pattern (Wong et al., 2007).

This near-regular five-spot pattern is represented by a 150 m by 150 m block to simulate the CO_2-ECBM pilot test, as shown in Fig. 3. The simulation model is shown in Fig. 4, in which the injection well (IW) is located at the lower left corner, and the production well (PW-1) is located at the top right corner. The well diameter is assumed as 0.1 m. For the coal deformation model, the left side and base are constrained and in situ stresses are applied to the top and the right sides. For the gas flow, a constant pressure of 0.1 MPa is applied to the production well. No flow conditions are applied to all the other boundaries. An initial pressure of 2.5 MPa is applied in the model, in which the CH_4 saturation is 85%. Input properties are listed in Table 1. The values of these properties were chosen from the literature (Mazumder et al., 2007; Shi et al., 2008; Wong et al., 2007). In all these simulations, the fracture spacing and opening are assumed as $a = 0.01$ m and $b = 10^{-5}$ m, respectively, the modulus ratio is assumed as $K_f/K = 0.1$ and the in situ stresses as $Fy = Fx = -6$ MPa. The simulation time is 10^4 days (about 30 years).

Three senarios are simulated to quantify the CO_2-enhanced gas recovery as shown in Table 2. The first model is to simulate the CBM production without the CO_2 injection. The other two models are for the CO_2-ECBM recovery under two injection pressures, 4 MPa and 8 MPa, respectively. CO_2 is injected in the injection well (IW) while gas is extracted through the production well (PW-1).

4.2. Simulation results

4.2.1. Distributions of pressures

Fig. 5 shows the distribution of the total pressure for three different simulation models. Fig. 6 shows the evolution of the partial pressure of each gas component in the fracture system at point B (50,50).

For CBM production without CO_2 injection the total pressure decreases continuously, as shown in Fig. 5 (Model 1) until it reaches a steady state, i.e., the total pressure in the reservoir is equal to the bottomhole pressure in the production well. For the CO_2-injection cases the total pressure gradient increases significantly because of the injection as shown in Fig. 5 (Model 2 and Model 3). For the partial pressures, CO_2 injection further lowers the methane pressure in the fracture system while the CO_2 pressure builds, as shown in Fig. 6. The non-linear build-up of CO_2 pressure is due to the differential swelling. The reduction in the CH_4 pressure is due to the enhancement of gas production.

4.2.2. Gas concentrations in the matrix system

Fig. 7 shows the distribution of CH_4 concentration in the matrix system. Without the injection of CO_2 the CH_4 content in the matrix changes very slowly and this change is confined to the vicinity of the production well. After producing for 1 year the gas content of CH_4 is 16.7%–70% within 5 m of the wellbore, and 82.3% beyond this radius which is almost the same as the initial state. This region extends to about 20 m from the well by 10 years. With CO_2 injection (model 2 and model 3) the area in which CH_4 content decreases begins directly

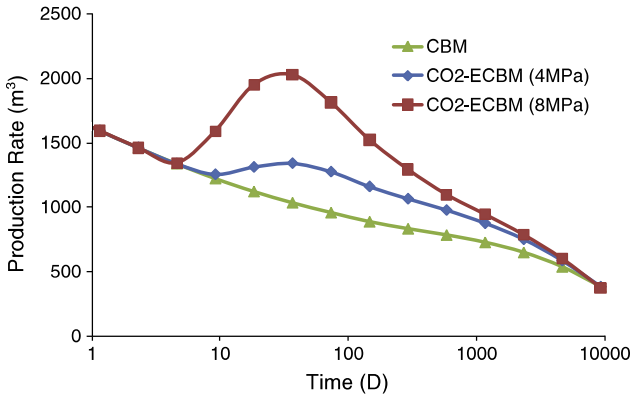

Fig. 9. CH_4 production rates for three different simulation models.

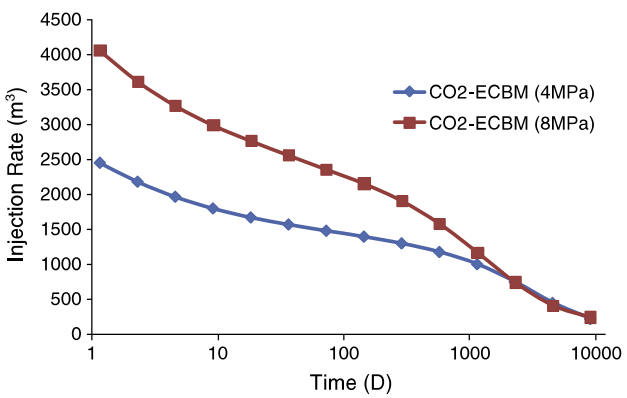

Fig. 11. Daily injection rate of CO_2 for the two models.

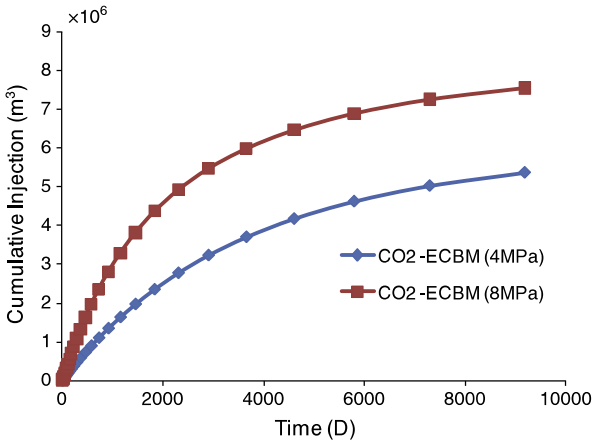

Fig. 12. Cumulative injection of CO_2 for the two models.

at the injection well. The larger the injection pressure the larger the area swept by CO_2 becomes.

Fig. 8 shows the evolution of CO_2 and CH_4 contents at point B in the matrix. The dashed lines represent the CO_2 content while the solid lines represent the CH_4 content. Without the CO_2 injection the CH_4 content decreases almost linearly but with CO_2 injection the CH_4 content decreases exponentially. When the injection pressure is 8 MPa it takes about 500 days before he CO_2 content outstrips the CH_4 content. If the injection pressure is lower, at 4 MPa, it takes correspondingly longer for the CO_2 and CH_4 pressures to become equivalent — about 6 years.

4.2.3. Gas production rate

Fig. 9 shows the rates of production CH_4 for three different simulation models. Without CO_2 injection the CH_4 production rate decreases almost linearly. With CO_2 injection the CH_4 production rate decreases linearly before the injection takes effect, and then increases significantly after the injection takes effect. Fig. 10 shows the CH_4 cumulative productions for the three different simulation models. It shows clearly that the CO_2 injection increases the cumulative CH_4 production. These simulation results are in agreement with the outcomes of the pilot testing (Wong et al., 2007).

4.2.4. CO_2 injection rate

Fig. 11 shows the CO_2 injection rate for two different simulation models. It is apparent that the initial injection rates are regulated by the injection pressure: the higher the injection pressure, the higher the CO_2 injection rate. Both injection rates decrease gradually. After about 2000 days, both injection rates are almost the same because

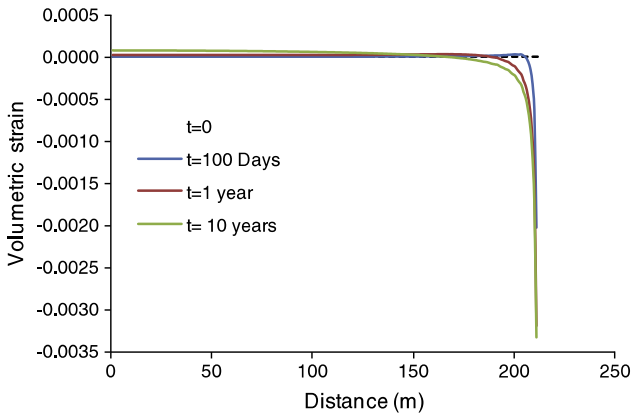

Fig. 13. Volumetric strain along the diagonal of model 1.

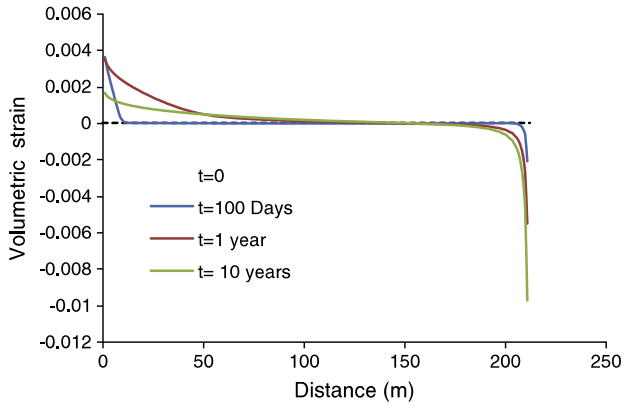

Fig. 14. Volumetric strain along the diagonal of model 2.

both cases have reached the minimum permeability. Fig. 12 shows the cumulative CO_2 injection for two different simulation models. Apparently, the total amount of CO_2 that is injected into the coal is proportional to the injection pressure.

4.2.5. Evolution of coal volumetric strain

Figs. 13–15 show the evolution of the volumetric strain along the diagonal line A–A′. Without CO_2 injection the volumetric strain near the production well is negative, representing shrinkage of the coal. This shrinkage results from the CH_4 desorption in the vicinity of the wellbore. As the CBM production progresses the area subject to shrinkage migrates outwards from the wellbore into the coal seam. This region expands to about 60 m from the well in 10 years. However, the volumetric strains near the injection well of the models

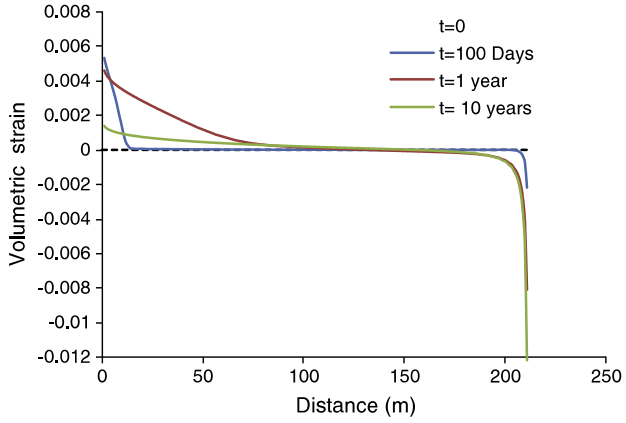

Fig. 15. Volumetric strain along the diagonal of model 3.

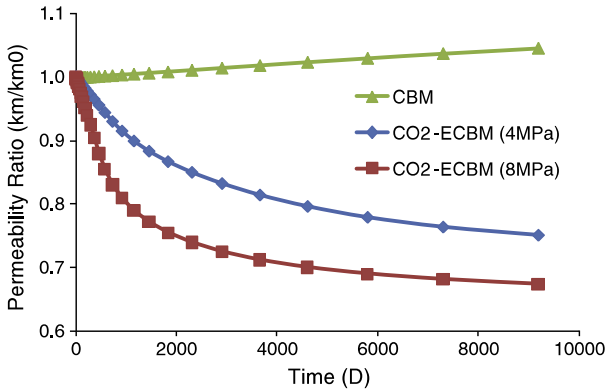

Fig. 16. Evolution of permeability ratios at point B in the matrix.

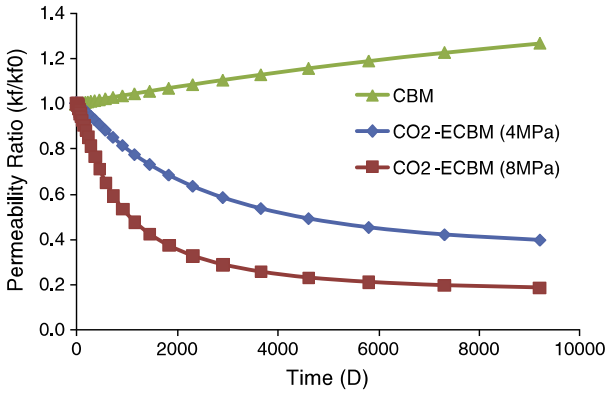

Fig. 17. Evolution of permeability ratios at point B in the fracture.

with the CO_2 injections are positive. This means that the coal in this area swells while the volumetric strain near the production well is still negative. As CO_2 injection progresses the zone of swelling moves outwards from the injection well into the coal seam while the magnitudes of induced swelling fluctuate.

4.2.6. Evolution of coal permeability

Figs. 16 and 17 show the evolutions of coal permeability at point B in the matrix and fracture systems, respectively. The trends of permeability changes in the matrix system are similar to those in the fracture system but their magnitudes are significantly different. Without CO_2 injection both matrix permeability and fracture permeability increase. With CO_2 injection both permeabilities decrease but the reductions in fracture permeability are much more dramatic than the reductions in the matrix permeability.

5. Conclusions

In this work, general porosity and permeability models are developed to explicitly quantify the interactions between binary gas mixtures (CO_2 and CH_4) and dual solid media (coal matrix and fracture) under the full spectrum of mechanical conditions spanning prescribed in-situ stresses through constrained displacement. These models are implemented into a fully coupled finite element (FE) model of coal deformation, binary gas flow and transport in the matrix system, and binary gas flow and transport in the fracture system. This model represents important non-linear responses due to the effective stress effects that cannot be recovered where mechanical influences are not rigorously coupled with the binary gas transport system.

The model is applied to represent the evolution of permeability when CH_4 is withdrawn and subsequently CO_2 is injected to enhance recovery. The results demonstrate the complexity of the CO_2-injection induced interactions between binary gases (CO_2 and CH_4) and dual solid media (coal matrix and fracture). This complexity cannot be captured without the full range of couplings included in this model.

Nomenclature

a	average length of matrix
b	average aperture of fracture
ε_{ij}	component of the total strain tensor
u_i	component of the displacement
σ_{ij}	component of the total stress tensor
f_i	component of the body force
ε_s	total sorption-induced strain
ε_{Lk}	sorption-induced strain of gas component k
b_k'	Langmuir pressure constant for gas component k
R	universal gas constant
T	absolute temperature
σ_{kk}	normal stress component
K	bulk modulus of coal
K_s	bulk modulus of coal grains
K_n	stiffness of coal fracture
G	shear modulus of coal
E	Young's modulus of coal
E_s	Young's modulus of coal grains
ν	Poisson ratio of coal
α	Biot coefficient of matrix
β	Biot coefficient of fracture
δ_{ij}	Kronecker delta (1 for $i=j$, 0 for $i\neq j$)
C_{mk}	concentration of gas component k in matrix
C_{fk}	concentration of gas component k in fracture
ρ_g	gas density
$\vec{q}_g$	vector of Darcy velocity
Q_s	gas source or sink
k_m	permeability of matrix
k_f	permeability of fracture
D_k	hydrodynamic dispersion coefficient
D_{k0}	molecular diffusion coefficient of gas component k
μ	dynamic viscosity of gas
M_k	molar mass of gas component k
ρ_{ga}	density of gas under standard condition
ρ_c	coal density
ϕ_m	porosity of matrix
ϕ_f	porosity of fracture
V_{Lk}	Langmuir volume constant of gas component k
ε_v	volumetric strain of coal
subscript 0	initial value of the variable
subscript m	matrix
subscript f	fracture

Acknowledgments

This work was supported by ConocoPhillips, the National Basic Research Program of China (2007CB209400), Chinese National Natural Science Foundation (50904065), and State Key Laboratory for Geomechanics and Deep Underground Engineering in China. The sources of this support are gratefully acknowledged.

References

Bai, M., Elsworth, D., 2000. Coupled processes in subsurface deformation. Flow and Transport. ASCE Press. 336 pp.

Bergen, F., et al., 2009. Production of gas from coal seams in the Upper Silesian coal basin in Poland in the post-injection period of an ECBM pilot site. International Journal of Coal Geology 77, 175–187.

Biot, M.A., 1941. General theory of three-dimensional consolidation. Journal of Applied Physics 12, 155–164.

Busch, A., Gensterblum, Y., Krooss, B.M., Littke, R., 2004. Methane and carbon dioxide adsorption–diffusion experiments on coal: upscaling and modeling. International Journal of Coal Geology 60, 151–168.

Butler, J.A.V., Ockrent, C., 1930. Studies in electrocapillarity. Part III. The surface tensions of solutions containing two surface-active solutes. Journal of Physics and Chemistry 34, 2841–2845.

Charrière, D., Pokryszk, Z., Behra, P., 2010. Effect of pressure and temperature on diffusion of CO_2 and CH_4 into coal from the Lorraine basin (France). International Journal of Coal Geology 81 (4), 373–380.

Chen, Z.W., Liu, J., Elsworth, D., Connell, L.D., Pan, Z., 2010. Impact of CO_2 injection and differential deformation on CO_2 injectivity under in-situ stress conditions. International Journal of Coal Geology 81 (2), 97–108.

Chikatamarla, L., Cui, X., Bustin, R.M., 2004. Implications of volumetric swelling/shrinkage of coal in sequestration of acid gases. International Coalbed Methane Symposium Proceedings, Tuscaloosa, Alabama, paper 0435.

Connell, L.D., Detournay, C., 2009. Coupled flow and geomechanical processes during enhanced coal seam methane recovery through CO_2 sequestration. International Journal of Coal Geology 77, 222–233.

Day, S., Fry, R., Sakurovs, R., 2008. Swelling of Australian coals in supercritical CO_2. International Journal of Coal Geology 74 (1), 41–52.

Detournay, E., Cheng, A.H.D., 1993. In: Fairhurst, C. (Ed.), Fundamental of poroelasticity. : Comprehensive Rock Engineering, Vol. II. Pergamon, Oxford, pp. 113–171.

Do, D.D., 1998. Adsorption Analysis: Equilibria and Kinetics. Imperial College Press, London.

Durucan, S., Shi, J.-Q., 2008. Improving the CO_2 well injectivity and enhanced coalbed methane production performance in coal seams. International Journal of Coal Geology 77, 214–221.
Elsworth, D., Bai, M., 1992. Flow-deformation response of dual porosity media. Journal of Geotechnical Engineering 118 (1), 107–124.
Fathi, E., Akkutlu, I.Y., 2008. Counter-diffusion and competitive adsorption effects during CO_2 injection and coalbed methane production. Society of petroleum engineers. SPE 115482.
Fokker, P.A., van der Meer, L.G.H., 2004. The injectivity of coalbed CO_2 injection wells. Energy 29, 1423–1429.
Fujioka, M., et al., 2010. CO_2-ECBM field tests in the Ishikari coal basin of Japan. International Journal of Coal Geology. doi:10.1016/j.coal.2010.01.004.
Goodman, A.L., Favors, R.N., Hill, M.M., Larsen, J.W., 2005. Structure changes in Pittsburgh No. 8 Coal caused by sorption of CO_2 gas. Energy and Fuels 19, 1759–1760.
Gray, I., 1992. Reservoir engineering in coal seams: Part 1 — The physical process of gas storage and movement in coal seams. Society of Petroleum Engineers, Reprint Series 35, 7–13.
Gunter, W.D., Gentzis, T., Rottenfuser, B.A., Richardson, R.J.H., 1997. Deep coalbed methane in Alberta, Canada: a fuel resource with the potential of zero greenhouse gas emissions. Energy Conversion and Management 38, 217–222.
Hall, F.E., Zou, C.H., Gasem, K.A.M., Robinson, R.L., Yee, D., 1994. Adsorption of pure methane, nitrogen, and carbon dioxide and their binary mixtures on wet Fruitland coal. SPE 29194-MS.
IPCC, 2005. IPCC Special Report on Carbon Dioxide Capture and Storage. Cambridge University Press, UK.
Karacan, C.O., 2003. Heterogeneous sorption and swelling in a confined and stressed coal during CO_2 injection. Energy Fuels 17, 1595–1608.
Karacan, C.O., 2007. Swelling-induced volumetric strains internal to a stressed coal associated with CO_2 sorption. International Journal of Coal Geology 72, 209–220.
Korre, A., Shi, J.Q., Imrie, C., Grattoni, C., Durucan, S., 2007. Coalbed methane reservoir data and simulator parameter uncertainty modeling for CO_2 storage performance assessment. International Journal of Greenhouse Gas Control 1 (4), 492–501.
Krooss, B.M., Van Bergen, F., Gensterblum, Y., Siemons, N., Pagnier, H.J.M., David, P., 2002. High-pressure methane and carbon dioxide adsorption on dry and moisture-equilibrated Pennsylvanian coals. International Journal of Coal Geology 51 (2), 69–92.
Kuuskraa, V.A., Boyer, J.N., 1992. Coalbed gas 1—hunt for quality basins goes abroad. Oil and Gas Journal, OGJ Special—Unconventional Gas. Development 5, 49–54.
Langmuir, I., 1916. The constitution and fundamental properties of solids and liquids, part I. Solids. Journal of the American Chemical Society 38, 2221–2295.
Larsen, J.W., 2003. The effects of dissolved CO_2 on coal structure and properties. International Journal of Coal Geology 57 (1), 63–70.
Levine, J.R., 1996. Model study of the influence of matrix shrinkage on absolute permeability of coal bed reservoirs. Geologic Society, London, Special Publication 109, 197–212.
Liu, J., Chen, Z., Elsworth, D., Miao, X., Mao, X., 2010a. Linking gas-sorption induced changes in coal permeability to directional strains through a modulus reduction ratio. International Journal of Coal Geology 83 (1), 21–30.
Liu, J., Chen, Z., Elsworth, D., Miao, X., Mao, X., 2010b. Evaluation of stress-controlled coal swelling processes. International Journal of Coal Geology. doi:10.1016/j.coal.2010.06.005.
Mazumder, S., Wolf, K.-H., 2007. Differential swelling and permeability change of coal in response to CO_2 injection for ECBM. International Journal of Coal Geology 74, 123–138.
Mazumder, S., Wolf, K.-H.A.A., Bruining, H., 2005. The relationship between coal macromolecular structure and its swelling. Proceedings International RECOPOL workshop Szcyrk (Poland).
Mazumder, S., Wolf, K.H.A.A., Van Hemert, P., Busch, A., 2007. Laboratory experiments on environmental friendly means to improve coalbed methane production by carbon dioxide/flue gas injection. Transport in Porous Media 75, 63–92.
Palmer, I., 2009. Permeability changes in coal: analytical modeling. International Journal of Coal Geology 77, 119–126.
Palmer, I., Mansoori, J., 1996. How permeability depends on stress and pore pressure in coalbeds: a new model. SPE-52607.
Pan, Z.J., Connell, L.D., 2009. Comparison of adsorption models in reservoir simulation of enhanced coalbed methane recovery and CO_2 sequestration in coal. International Journal of Greenhouse Gas Control 3, 77–89.
Pekot, L.J., Reeves, S.R., 2002. Modeling the effects of matrix shrinkage and differential swelling on coalbed methane recovery and carbon sequestration. U.S. Department of Energy DE-FC26-00NT40924.
Pone, J.D.N., Hile, M., Halleck, P.M., Mathews, J.P., 2008. Three-dimensional carbon dioxide-induced strain distribution within a confined bituminous coal. International Journal of Coal Geology 77, 103–108.
Prusty, B.K., 2007. Sorption of methane and CO_2 for enhanced coalbed methane recovery and carbon dioxide sequestration. Journal of Natural Gas Chemistry 17, 29–38.
Robertson, E.P., Christiansen, R.L., 2005. Measurement of sorption-induced strain. International Coalbed Methane Symposium, University of Alabama, Tuscaloosa. Paper 0532.
Robertson, E.P., Christiansen, R.L., 2007. Modeling laboratory permeability in coal using sorption-induced-strain data. SPE Reservoir Evaluation & Engineering 10 (3), 260–269.
Seidle, J.P., Huitt, L.G., 1995. Experimental measurements of coal matrix shrinkage due to gas desorption and implications for cleat permeability increases. SPE-30010-MS.
Shi, J.-Q., Durucan, S., 2004. A numerical simulation study of the Allison unit CO_2-ECBM pilot: the impact of matrix shrinkage and swelling on ECBM production and CO_2 injectivity. Proceedings of 7th International Conference on Greenhouse Gas Control Technologies.
Shi, J.-Q., Durucan, S., 2005. A model for changes in coalbed permeability during primary and enhanced methane recovery. SPE Reservoir Evaluation & Engineering 8 (4), 291–299.
Shi, J.-Q., Durucan, S., 2008. Modeling of mixed-gas adsorption and diffusion in coalbed reservoirs. SPE 114197.
Shi, J.-Q., Mazumder, S., Wolf, K.-H., Durucan, S., 2008. Competitive methane desorption by supercritical CO_2 injection in coal. Transport in Porous Media 75, 35–54.
Siemons, N., Busch, A., 2007. Measurement and interpretation of supercritical CO_2 sorption on various coals. International Journal of Coal Geology 69 (4), 229–242.
Stauffer, P.H., Viswanathan, H.S., Pawar, R.J., Guthrie, G.D., 2009. A system model for geologic sequestration of carbon dioxide. Environmental Science & Technology 43 (3), 565–570.
Stevens, S.H., Kuuskraa, V.A., Spector, D., Riemer, P., 1999. CO_2 sequestration in deep coal seams: pilot results and worldwide potential. Proceedings of the 4th International Conference on Greenhouse Gas Control Technologies, Interlake, Switzerland, pp. 175–180.
Su, X., et al., 2005. Geology of coalbed methane reservoirs in the Southeast Qinshui Basin of China. International Journal of Coal Geology 62 (4), 197–210.
Wang, G.X., Massarottoa, P., Rudolpha, V., 2009. An improved permeability model of coal for coalbed methane recovery and CO_2 geosequestration. International Journal of Coal Geology 77, 127–136.
Wei, X.R., Wang, G.X., Massarotto, P., Golding, S.D., Rudolph, V., 2007. Numerical simulation of multicomponent gas diffusion and flow in coals for CO_2 enhanced coalbed methane recovery. Chemical Engineering Science 62 (16), 4193–4203.
White, C.M., Smith, D.H., Jones, K.L., et al., 2005. Sequestration of carbon dioxide in coal with enhanced coalbed methane recovery, a review. Energy and Fuels 19 (3), 659–724.
Wong, S., Law, D., Deng, X., et al., 2007. Enhanced coalbed methane and CO_2 storage in anthracitic coals-Micro-pilot test at South Qinshui, Shanxi, China. International Journal of Greenhouse Gas Control 1, 215–222.
Wong, S., et al., 2010. Conceptual economics of full scale enhanced coalbed methane production and CO_2 storage in anthracitic coals at South Qinshui basin. International Journal of Coal Geology. doi:10.1016/j.coal.2010.01.011.
Wu, Y., Liu, J., Chen, Z., et al., 2009. Dual poroelastic response of coal seam to CO_2 injection. 43rd U.S. Rock Mechanics Symposium and 4th U.S.-Canada Rock Mechanics Symposium, Asheville, NC June 28th–July 1.
Wu, Y., Liu, J., et al., 2010. Dual poroelastic response of a coal seam to CO_2 injection. International Journal of Greenhouse Gas Control 4 (4), 668–678.
Yi, J., Akkutlu, I.Y., Deutsch, C.V., 2008. Gas transport in bidisperse coal particles: investigation for an effective diffusion coefficient in coalbeds. Journal of Canadian Petroleum Technology 47 (10), 20–26.
Zhang, H.B., Liu, J., Elsworth, D., 2008. How sorption-induced matrix deformation affects gas flow in coal seams: a new FE model. International Journal of Rock Mechanics and Mining Sciences 45 (8), 1226–1236.